analytical chemistry

pubs.acs.org/ac Article

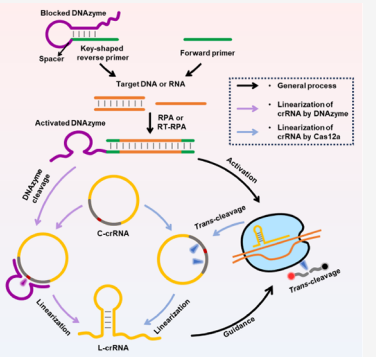
DNAzyme-Triggered Equilibrium Transfer with Self-Activated CRISPR-Cas12a Biosensor Enables One-Pot Diagnosis of Nucleic Acids

Di Huang, Yichen He, Chutian Xu, Peijie Shen, Min Li, Mengjun Fang, Zhinan Xu,* and Xiangming Fang*

Cite This: *Anal. Chem.* 2025, 97, 3026−3035 Read Online

ACCESS | Metrics & More | Article Recommendations | Supporting Information

ABSTRACT: Integrating recombinase-polymerase amplification (RPA) with CRISPR-Cas12a holds significant potential to simplify and improve nucleic acid diagnostic procedures. However, current strategies face limitations, such as complexity, reduced efficiency, and potential compromises in Cas12a activity. In response, we developed a DNAzyme-triggered equilibrium transfer with a self-activated CRISPR-Cas12a biosensor (DESCRIBER) for integrated nucleic acid detection. This platform features varying balance points to minimize interference between RPA and Cas12a in one pot and maximize their activity at different stages. Initially, the reaction focused on RPA, while Cas12a was silenced by circular-crRNA (C-crRNA). Then, DNAzyme, the activator, was generated during the RPA process, which linearizes C-crRNA to activate Cas12a and transfer the equilibrium toward signal readout. Meanwhile, activated Cas12a can further linearize C-crRNA to promote self-activation and accelerate equilibrium transfer. According to this principle, highly sensitive detection of the HIV-1 genome, as low as 500 CPs/mL, was achieved within 1 h while maintaining universality in detecting common subtypes and specificity against opportunistic infectious pathogens. Compared with qRT-PCR, it also exhibited good accuracy in detecting 35 spiked samples. Overall, we believe that the proposed strategy will enhance existing CRISPR systems to promote their practical applications in clinical diagnosis.

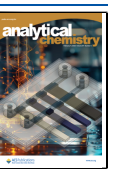


INTRODUCTION

The clustered regularly interspaced short palindromic repeats (CRISPR) with its associated protein (Cas) is an emerging and promising biotechnological tool.[1,2] CRISPR-Cas was initially developed and applied as a gene-editing tool and has now rapidly evolved into a highly prevailing technology for *in vitro* diagnosis of nucleic acid.[3−6] Triggered by CRISPR RNA (crRNA), the representative CRISPR-Cas12a could accurately recognize target DNA and subsequently activate its specific *cis*-cleavage at the target double-stranded DNA (dsDNA), as well as the nonspecific *trans*-cleavage at sequence-unrelated single-stranded DNA (ssDNA).[7−9] Because of these special enzymatic activities, several nucleic acid detection platforms have been established based on CRISPR-Cas12a, such as DNA endonuclease-targeted CRISPR trans reporter (DETECTOR)[10] and one-HOur Low-cost Multipurpose highly Efficient System (HOLMES).[11] These detection systems normally rely on nucleic acid amplification techniques to enhance the preliminary signal and thus achieve ultrahigh sensitivity, and recombinase-polymerase amplification (RPA) is usually applied due to its isothermal compatibility with Cas12a.[12,13] However, this two-step reaction mode with the transfer of amplification product often complicates the detection process and raises the risk of aerosol contamination-induced false positives.[14,15]

Many efforts have been devoted to improving the Cas12a-based detection systems. Although two reaction steps could be integrated within one chamber, nucleic acid templates and primers might be disrupted by the *trans*-cleavage of Cas12a, thereby impairing amplification efficiency and detection sensitivity.[16,17] Subsequent approaches such as weakening the activity or delaying the activation of Cas12a have been adopted to improve the compatibility between steps. Depending on the manner in which RPA and Cas12a initially separate, these methods can be categorized into spatial and temporal separation strategies. For spatial separation, two systems are completely separated by utilizing either rigid setups, such as microfluidic chips or specially designed devices,[18−20] or flexible setups, such as membranes,[21] double water-phase interfaces,[22,23] or hydrogel interfaces.[24] Following RPA amplification, rigid setups facilitate material exchange between chambers through active forces such as centrifugation or magnetism.

Received: November 10, 2024
Revised: January 22, 2025
Accepted: January 23, 2025
Published: January 31, 2025



Downloaded via SHANGHAI NORMAL UNIV on February 19, 2025 at 01:23:13 (UTC).
See https://pubs.acs.org/sharingguidelines for options on how to legitimately share published articles.

ACS Publications © 2025 American Chemical Society

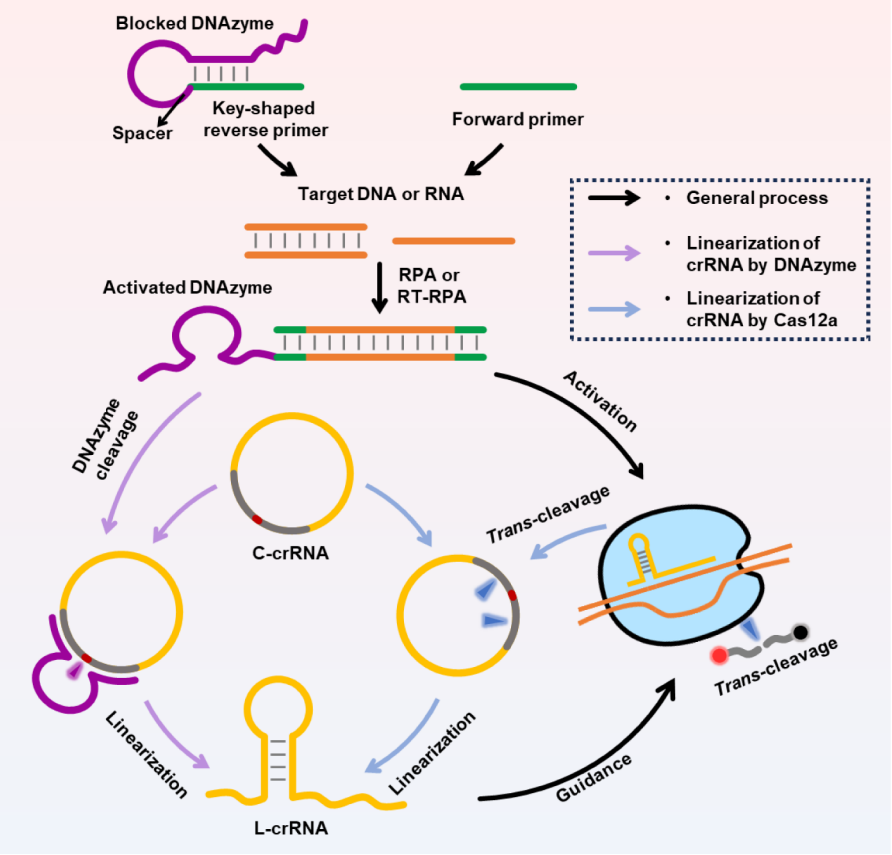


Figure 1. Working principle of DNAzyme-triggered equilibrium transfer with a self-activated CRISPR-Cas12a biosensor (DESCRIBER) for the integrated nucleic acid detection.

Despite their integration in reaction form, RPA and Cas12a remain temporally independent processes. This strategy does not significantly boost detection efficiency fundamentally and requires extra instruments. Conversely, flexible setups enable RPA products to cross interfaces via diffusion and then activate the Cas12a system. However, the control of diffusion force is challenging and may slow response time and affect detection efficiency.[3]

In the temporal separation strategies, RPA and Cas12a are thoroughly mixed, but the latter is blocked or weakened via different silence targets, including Cas12a silence, crRNA silence, and complex silence. Cas12a silence uses an anti-Cas protein with an affinity for Cas12a to temporarily enclose its activity,[25] which can be timely reversed through protein hydrolysis. Similarly, crRNA silence utilizes photosensitive molecules to prevent crRNA from binding with Cas12a, which can be timely reversed through light-responsive reactions.[26−28] The reaction-driven strategies described above also face challenges similar to those of rigid spatial separation. Complex silence adopts dsDNA with a suboptimal protospacer adjacent motif (PAM)[29] or PAM-lacking ssDNA[30] as recognition targets, but the sacrifice of Cas12a enzymatic activity could potentially cause a loss of sensitivity.

Consequently, the available integrating strategies still showed inconvenience or reduced efficiency and thus cannot resolve the compatibility issues between RPA and Cas12a. To address these concerns, we developed a self-activated and integrated nucleic acid detection platform that could simultaneously process both steps without compromising the activity of Cas12a. Initially, Cas12a was temporarily silenced, and the RPA process was promoted to generate amplicons and activators. Then, these activators released Cas12a and enabled it to identify the amplicons with the trigger of crRNA, so the activation of *trans*-cleavage activity shifted the equilibrium toward signal readout. A key feature of this method was the varied balance points at different stages, which kept the minimal interference between RPA and Cas12a during their respective dominant phases. Additionally, the transition of equilibrium was driven by a self-activated force from the activators, which was intensified with the progress of this reaction and expedited the equilibrium transfer. Finally, a DNAzyme-triggered equilibrium transfer with a self-activated CRISPR-Cas12a biosensor (DESCRIBER) was developed for integrated nucleic acid detection, and the potential of DESCRIBER in *in vitro* diagnosis was evaluated using human immunodeficiency virus-1 (HIV-1) as a model target.

EXPERIMENTAL SECTION

Characterization of Interactions between Different crRNAs and Cas12a. The binding affinities of Cas12a for L-crRNA, C-crRNA, and C-crRNA treated with DNAzyme were measured by a time-resolved fluorescence anisotropy analysis. A 100 μL testing system consisted of 1× binding buffer (50 mM NaCl, 10 mM Tris-HCl, 10 mM $MgCl_2$, 1 mM DTT, 5% glycerol, 50 μg/mL heparin, 50 μg/mL recombinant albumin, pH 7.9), 5 nM FAM-labeled crRNA (linear crRNA (L-crRNA), circular-crRNA (C-crRNA), reborn L-crRNA (C-crRNA treated by DNAzyme)), different concentrations of Cas12a, and 50 U RNase inhibitor. After incubation at 37 °C for 30 min to reach a steady state, the fluorescence anisotropy

https://doi.org/10.1021/acs.analchem.4c06066
Anal. Chem. 2025, 97, 3026−3035

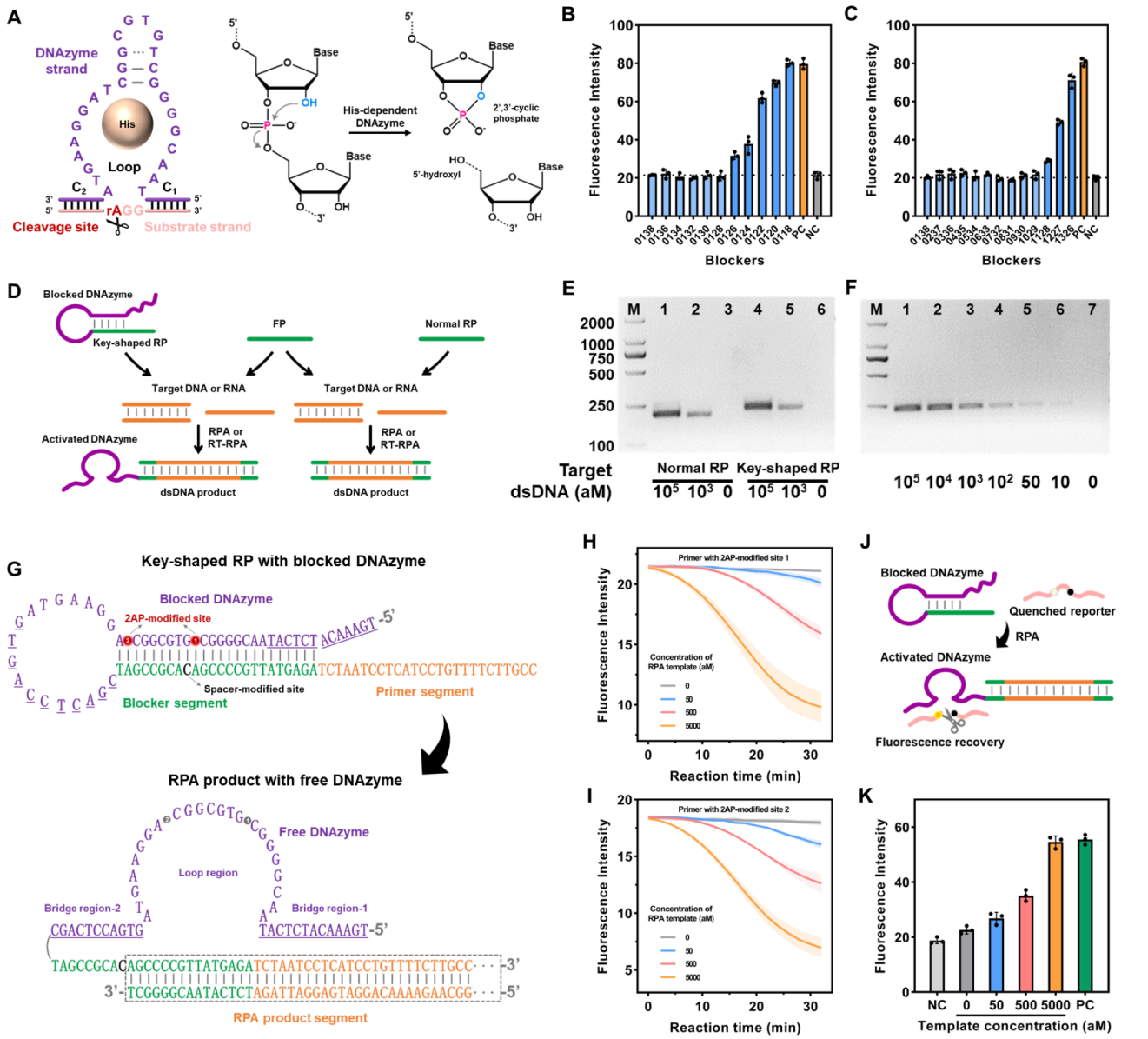


Figure 2. Effect of blocking and RPA-induced uncloaking of DNAzyme. (A) Cleavage mechanism of the His-dependent DNAzyme used in this article. (B, C) Evaluation of the efficiency of blockers designed by different lengths and positions of cDNA of the DNAzyme (PC: positive control with the absence of any blockers; NC: negative control with the absence of DNAzyme). (D) Schematic of RPA using either self-blocking key-shaped RP or normal RP (FP: forward primer; RP: reverse primer). (E, F) Agarose gel electrophoresis analysis of RPA amplicons using a key-shaped RP or normal RP in the presence/absence of mimic target dsDNA as a template. (G) Schematic of the conformational changes of the key-shaped RP before and after the RPA process. (H, I) Characterization of the structural dynamics of the key-shaped RP during the RPA process. (J) Schematic of the DNAzyme restoring its normal conformation through the RPA process and the subsequent cleavage of the substrate reporter labeled with fluorophore and quencher. (K) Evaluation of the feasibility of RPA-induced uncloaking of DNAzyme.

values were measured by a microplate reader (λ_{Ex}: 485 nm, λ_{Em}: 520 nm). Subsequently, the K_d values were calculated by the fluorescence anisotropy change using the nonlinear fitting with the "one site-specific binding equation".

Detection Procedure of Fluorescence Assay Based on DESCRIBER. A 50 μL optimized fluorescence assay based on DESCRIBER was composed of 25 μL of Part A (essential enzymes of RT-RPA, 2 mM dNTPs, 6 mM ATP, and 160 mM His in 25 μL reaction buffer), 5 μL of Part B (2.5 μL 10 μM forward primer and 2.5 μL 10 μM key-shaped reverse primer), 10 μL of Part C (1 μL 10 μM LbCas12a, 2.5 μL 4 μM crRNA, 1.5 μL 40 U/μL RNase inhibitor, 2.5 μL 20 μM fluorescence reporter, and 2.5 μL activation buffer), and 10 μL of Part D (10 μL extracted sample). To be specific, solid components were first dissolved in 25 μL of reaction buffer to prepare Part A. Then, it was thoroughly mixed with Part B and Part D. Finally, Part C was immediately added and thoroughly mixed again, followed by incubation at 37 °C in 384-well plates. The fluorescence signal of each test was measured by a Varioskan Flash Multimode Plate Reader from Thermo Fisher Scientific Co., Ltd. (Waltham, USA) every 2 min.

Detection Procedure of Test Strip Assay Based on DESCRIBER. A 50 μL optimized test strip assay based on DESCRIBER possessed a composition essentially identical to that of the fluorescence assay, except that the test strip reporter was used instead of the fluorescence reporter. The reaction was

https://doi.org/10.1021/acs.analchem.4c06066
Anal. Chem. 2025, 97, 3026−3035

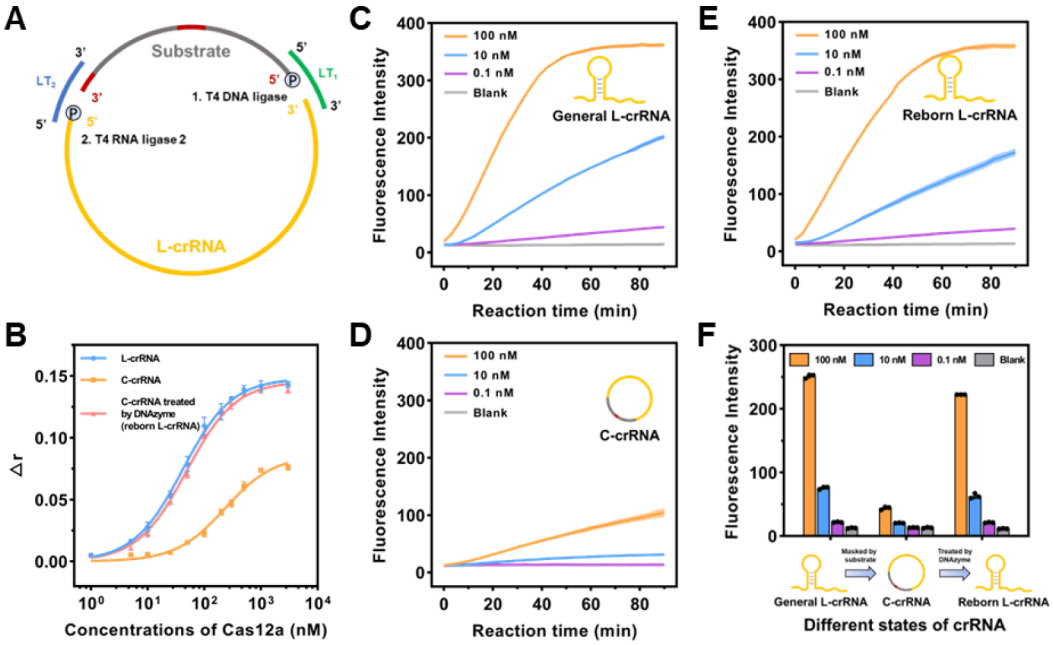


Figure 3. Characterization of interactions between different crRNAs and Cas12a. (A) Schematic of the C-crRNA preparation method using a one-step reaction based on dual padlock probes. (B) Characterization of the binding affinity of Cas12a for L-crRNA, C-crRNA, and C-crRNA treated by DNAzyme using the time-resolved fluorescence anisotropy analysis. (C−E) Fluorescence kinetic analysis using normal Cas12a fluorescence assay with L-crRNA, C-crRNA, and reborn L-crRNA, respectively, in the absence or presence of mimic target dsDNA. (F) Evaluation of the impact of different types of crRNA on the *trans*-cleavage activity of Cas12a. The fluorescence intensity was measured after 30 min of reaction.

performed in a tube, and the sample was incubated at 37 °C for 1 h. Subsequently, 20 μL of the reaction solution was mixed with 80 μL of diluent buffer (0.05% Tween 20). Then, the strip was vertically placed into this solution and incubated at room temperature for 5 min. Finally, the strip was removed from the tube, followed by a signal readout by the naked eye or a smartphone. The test line intensity in the image was further analyzed by using ImageJ.

Data Analysis and Statistics. Experiments in each group were run in three technical replicates ($n = 3$). Reaction kinetics curves represented means (bold line) ± SD (area fill). The points in histograms represented individual measurements, and the error bars indicate ±SD. The test strip images were analyzed with ImageJ. Student's *t*-test was carried out using GraphPad Prism with a *P*-value <0.05 considered as statistically significant.

RESULTS AND DISCUSSION

Working Principle of DESCRIBER. The working principle of DESCRIBER for integrated nucleic acid detection is illustrated in Figure 1. In this system, circular-crRNA (C-crRNA) was adopted to silence Cas12a because of its much lower affinity for Cas12a, and this strategy set the initial balance of the reaction toward RPA or reverse transcription RPA (RT-RPA). On the other hand, a DNAzyme sequence segment (purple strand) was incorporated into one amplification primer and was self-blocked via intramolecular hybridization. In the presence of the target nucleic acids, abundant dsDNA targets (amplicons) were generated during RT-RPA. Meanwhile, the initially blocked DNAzyme gradually resumed its normal conformation (activators) through the strand displacement function of the DNA polymerase. With the assistance of histidine (His), the DNAzyme specifically linearized the ribonucleotide residue (red point) in the substrate region (gray strand) of C-crRNA. The resulting linear crRNA (L-crRNA) guided Cas12a to recognize the dsDNA target, activating its *trans*-cleavage activity and initiating the transfer of reaction equilibrium. The activated Cas12a not only, in turn, cleaved the substrate region of C-crRNA to release more L-crRNA and hasten the equilibrium transfer but also cleaved the reporters in fluorescence or test strip assays to achieve a dual-mode signal readout. Our system allowed the flexible integration of RT-RPA and Cas12a systems within a single chamber and thus created a "sample in, result out" nucleic acid detection platform without the need for additional driving forces.

Effect of Blocking and RPA-Induced Uncloaking of DNAzyme. The cleavage mechanism of the His-dependent DNAzyme was similar to that of the protein RNase A and is illustrated in Figure 2A. In a free system, the DNAzyme hybridized with its substrate strand to form a complex, which includes two complementary regions (C_1 and C_2) and a loop-like secondary structure. The imidazole group of the His cofactor functioned like a general base for the deprotonation of the 2' hydroxyl group near the cleaved phosphodiester bond.[31] As shown in Figures S1 and S2, the activity of the His-dependent DNAzyme was systematically characterized at the reaction temperature of RPA and Cas12a (37 °C), and it was confirmed that neither His nor the DNAzyme significantly interfered with the two reactions, making it suitable for establishing "one-pot" detection systems.

Since the activity of DNAzyme should be silenced before the RPA reaction, different lengths and positions of complementary DNA (cDNA) of the DNAzyme were designed as blockers (Figure S3). The hybridized strands of DNAzyme and blockers were mixed with the substrate reporter, and the reaction proceeded in the presence of His. After 1 h, the fluorescence signal generated by the reaction was recorded. As shown in Figure 2B,C, blockers 0138−0128 and 0138−1029 all effectively silenced the DNAzyme. Besides, the molecular

https://doi.org/10.1021/acs.analchem.4c06066
Anal. Chem. 2025, 97, 3026−3035

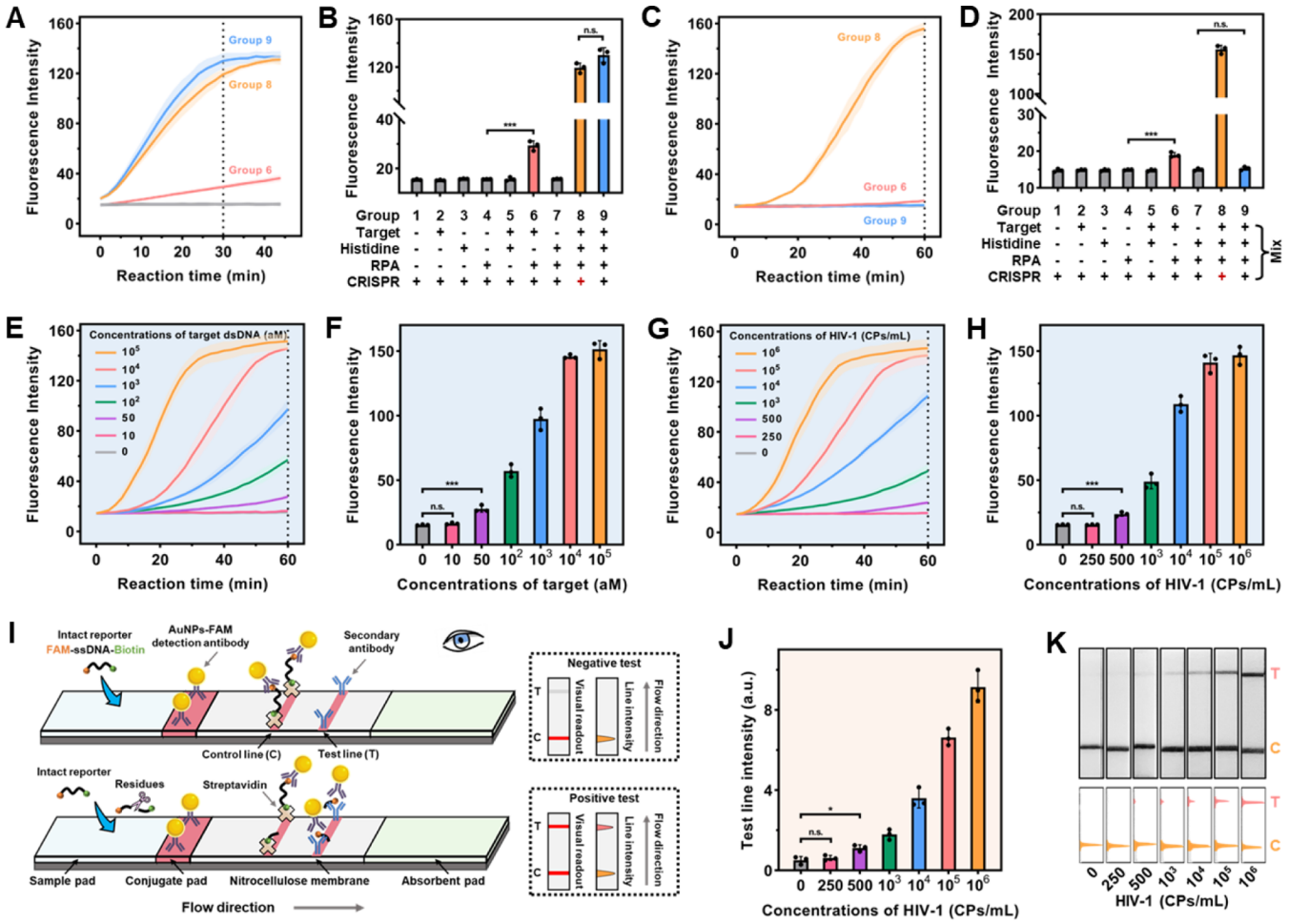


Figure 4. Feasibility and sensitivity characterization of DESCRIBER for HIV-1 detection. (A, B) Feasibility to replace L-crRNA with C-crRNA in the two-step RT-RPA-Cas12a system, which involved RT-RPA-induced uncloaking of DNAzyme, linearization of C-crRNA by DNAzyme, and Cas12a fluorescence assay. The histogram depicted the fluorescence intensity of each group measured after 30 min of the Cas12a fluorescence assay. The CRISPR-Cas12a systems in groups 8 and 9 contain C-crRNA treated by DNAzyme (reborn L-crRNA) and L-crRNA, respectively. (C, D) Feasibility of fluorescence assay based on DESCRIBER for "one-pot" detection of mimic target dsDNA. The histogram depicted the fluorescence intensity of each group measured after a total of 1 h of reaction. The CRISPR-Cas12a systems in groups 8 and 9 contain C-crRNA and L-crRNA, respectively. (E, G) Reaction kinetics of detecting different concentrations of mimic target dsDNA or HIV-1 genome using a fluorescence assay based on DESCRIBER. (F, H) Fluorescence intensity measured in each group after 1 h of reaction using a fluorescence assay based on DESCRIBER to evaluate its sensitivity in nucleic acid detection. (I) Working principle of the test strip assay based on DESCRIBER. (J, K) Evaluation of the sensitivity of the test strip assay based on DESCRIBER for HIV-1 detection, in which the pink peak indicated T line intensity, and the yellow one indicated that of the C line. The histogram depicted the quantification of T line intensity analyzed using ImageJ.

binding interactions between DNAzyme and blockers (1326−0732) were more thoroughly characterized in Figure S4 using native polyacrylamide gel electrophoresis. Considering the possible leakage of DNAzyme and its unfolding flexibility of the secondary structure, blocker 0831 was chosen for the subsequent research.

As illustrated in Figure 2D,G, a self-blocking key-shaped reverse primer (RP) for RPA was designed by successively connecting the end of the DNAzyme, blocker 0831, and normal RP sequences. A spacer-modified site was introduced within the blocker sequence to prevent excessive extension during RPA, thus ensuring proper reverse primer. Figure 2E,F demonstrated that the key-shaped RP, compared to the normal RP, did not significantly affect the RPA performance and could detect target dsDNA at concentrations as low as 10 aM.

To characterize the structural dynamics of the key-shaped RP during the RPA process, two 2-aminopurine-modified sites (2AP) were integrated into the DNAzyme sequence, positioned at the 3′ (2AP-1) and 5′ (2AP-2) ends of the spacer, respectively, as depicted in Figure 2G. As RPA progressed, a significant decrease in fluorescence signals was observed at both the 2AP-1 and 2AP-2 sites. This fluorescence reduction was intensified with the increase in RPA template concentration, suggesting the unwinding of the DNAzyme and the blocker during this process (Figure 2H,I). Subsequently, the RPA products were mixed with His and substrate reporter for reaction. The results in Figure 2K demonstrated a gradual increase in fluorescence signals with the increase in RPA template concentration, which further substantiated the restoration of normal cleavage activity as the DNAzyme transitioned from a blocked state.

Characterization of Interactions between Different crRNAs and Cas12a. C-crRNA was prepared in a one-step reaction using dual padlock probes (LT1 and LT2), where 5′-phosphorylated L-crRNA and the His-dependent DNAzyme

https://doi.org/10.1021/acs.analchem.4c06066
Anal. Chem. 2025, 97, 3026−3035

substrate were ligated by T4 DNA ligase and T4 RNA ligase 2, as described in Figure S5.

Using time-resolved fluorescence anisotropy analysis, the binding affinity of Cas12a for L-crRNA, C-crRNA, and C-crRNA treated by DNAzyme (the reborn L-crRNA) was measured (Figure 3B). The results revealed that L-crRNA exhibited strong binding affinity to Cas12a, with a K_d value of 41.56 ± 3.84 nm, while C-crRNA showed significantly reduced affinity, with a K_d of 234.25 ± 33.85 nm, representing an approximately 5.6-fold decrease in affinity, which was consistent with the reported literature.[32] Furthermore, the linearization of C-crRNA after treatment with DNAzyme restored its K_d to a level comparable to that of L-crRNA. Subsequently, L-crRNA, C-crRNA, and reborn L-crRNA were individually introduced into the conventional Cas12a fluorescence assay. As shown in Figure 3C−F, Cas12a mediated by L-crRNA or reborn L-crRNA exhibited a similar response to target dsDNA at the same concentration, while that of C-crRNA showed a significant attenuation. These findings demonstrated that the cyclization of crRNA disrupted its interaction with Cas12a and silenced Cas12a, while DNAzyme treatment linearized C-crRNA and thus relieved crRNA silence and restored Cas12a cleavage activity.

Establishment and Characterization of DESCRIBER. Next, the RPA and Cas12a reaction units were integrated and evaluated using HIV-1 as a model target. Based on our previous work, a relatively conserved detection region was identified in the *pol* fragment containing the central polypurine tract/central termination sequence (cPPT/CTS) element through sequence alignment of numerous HIV-1 subtypes from the Los Alamos National Laboratory database.[19] As shown in Figures S6−S7, six primer pairs were designed from the detection region, and F6R2, which exhibited high amplification efficiency and minimal nonspecific amplification, was selected for further experiments. When combined with RT-RPA, Cas12a, guided by L-crRNA, specifically recognized the amplicon, activating *trans*-cleavage and generating a significant fluorescence signal, thereby demonstrating its potential for HIV-1 detection.

To verify the feasibility of DESCRIBER, we first attempted to replace L-crRNA with C-crRNA in the two-step RT-RPA-Cas12a system. The process involved RT-RPA-induced release of DNAzyme, linearization of C-crRNA to reborn L-crRNA by DNAzyme, and the Cas12a fluorescence assay. As shown in Figure 4A,B, the final fluorescence assay triggered by L-crRNA (group 9) and reborn L-crRNA (group 8) both produced significant fluorescence signals in the presence of the HIV-1 genome, with minimal differences in the kinetic curves. In contrast, the assay triggered by C-crRNA (group 6) alone generated only a weak signal due to the residual affinity of C-crRNA for Cas12a shown in Figure 3. When the two-step RT-RPA-Cas12a system was integrated into DESCRIBER, the system with L-crRNA (group 9) did not produce a significant fluorescence signal (Figure 4C,D). However, the use of C-crRNA (group 8) enhanced the compatibility of the two systems, resulting in a substantial fluorescence signal. Interestingly, the absence of His in group 6 prevented the linearization of C-crRNA, reducing Cas12a activity and its interference with RT-RPA, thus producing a detectable fluorescence signal.

DESCRIBER with Dual-Mode Signal Readout for HIV-1 RNA Assay. After the feasibility of the DESCRIBER concept was validated, the analytical sensitivity of the fluorescence assay based on DESCRIBER was further assessed by detecting mimic targets (Figure 4E ,F). Ten aM dsDNA was undetectable even after extending the reaction time to 1 h, while an evident fluorescence signal was observed when the concentration of dsDNA was over 50 aM, and the fluorescence signal intensified progressively with the further increase of dsDNA concentration. Based on the kinetic analysis in Figure S8, at high concentrations of dsDNA, the reaction exhibited three distinct phases: lag phase, linear phase, and depletion phase. During the linear phase, the reaction rate remained relatively constant, tending toward a zero-order kinetic model. However, at lower concentrations of dsDNA, the reaction remained in the unsaturated Cas12a lag phase throughout the testing period. On the other hand, the fluorescence assay based on DESCRIBER could recognize as low as 500 CPs/mL HIV-1 genomes within 1 h, and a significant detectable signal was generated within 30 min when the concentration of HIV-1 genomes was higher than 10^3 CFU/mL (Figure 4G,H). Therefore, this method showed a sensitivity comparable to that of the two-step RT-RPA-Cas12a system, and it streamlined experimental procedures by eliminating the transfer of samples, thus reducing the risk of aerosol contamination.

The point-of-care testing (POCT) of HIV provides rapid results and has a wide range of applications, making it useful for the auxiliary early diagnosis of HIV-1 infection, monitoring disease progression, and evaluating the effectiveness of antiretroviral therapy. Therefore, a test strip assay based on DESCRIBER was also established, and it allowed nonprofessionals to perform tests after proper training without the dependence on large instruments and the requirements for specialized operations of fluorescence assays. As shown in Figure 4I, the ssDNA labeled with both FAM and biotin was served as the test strip reporter. In the absence of the dsDNA target, the intact reporter formed a complex with anti-FAM antibodies at the conjugate pad and was then captured by streptavidin in the control line (C), resulting in a color change due to the aggregated colloidal gold. In contrast, the test line (T) without passing through of the complex remained unchanged in color. In the presence of the target, Cas12a cleaved the reporter into two parts labeled with FAM or biotin, respectively. After the C line integrated the biotin part with streptavidin, the remaining FAM part with its antibodies was then captured by the secondary antibodies in the T line, causing this zone to turn red. Consequently, the red T line signified positive results, which could be easily observed with the naked eye or a portable strip reader. As shown in Figure 4J,K, the color change of the T line was intensified with the increase of HIV-1 genome concentration, enabling the visual detection of as low as 500 CPs/mL HIV-1 genome in 1 h. Besides, the gradation of the T line, as analyzed by ImageJ, also exhibited consistent results with visual observation, and the detection sensitivity was close to that of the fluorescence assay.

According to the National Guideline for Detection of HIV/AIDS in China (2020), the concentration threshold for the preliminary diagnosis of HIV-1 is 5000 CPs/mL. Therefore, both the fluorescence assay and test strip assay based on DESCRIBER could meet clinical testing requirements since their limits of detection (LODs) were improved and lower than the clinical threshold. The DESCRIBER-based POCT was practically valuable for the early diagnosis of HIV, reducing the need for extra tests and avoiding waste of healthcare resources, which could potentially boost the survival rates of infected individuals. Moreover, the development of

https://doi.org/10.1021/acs.analchem.4c06066
Anal. Chem. 2025, 97, 3026−3035

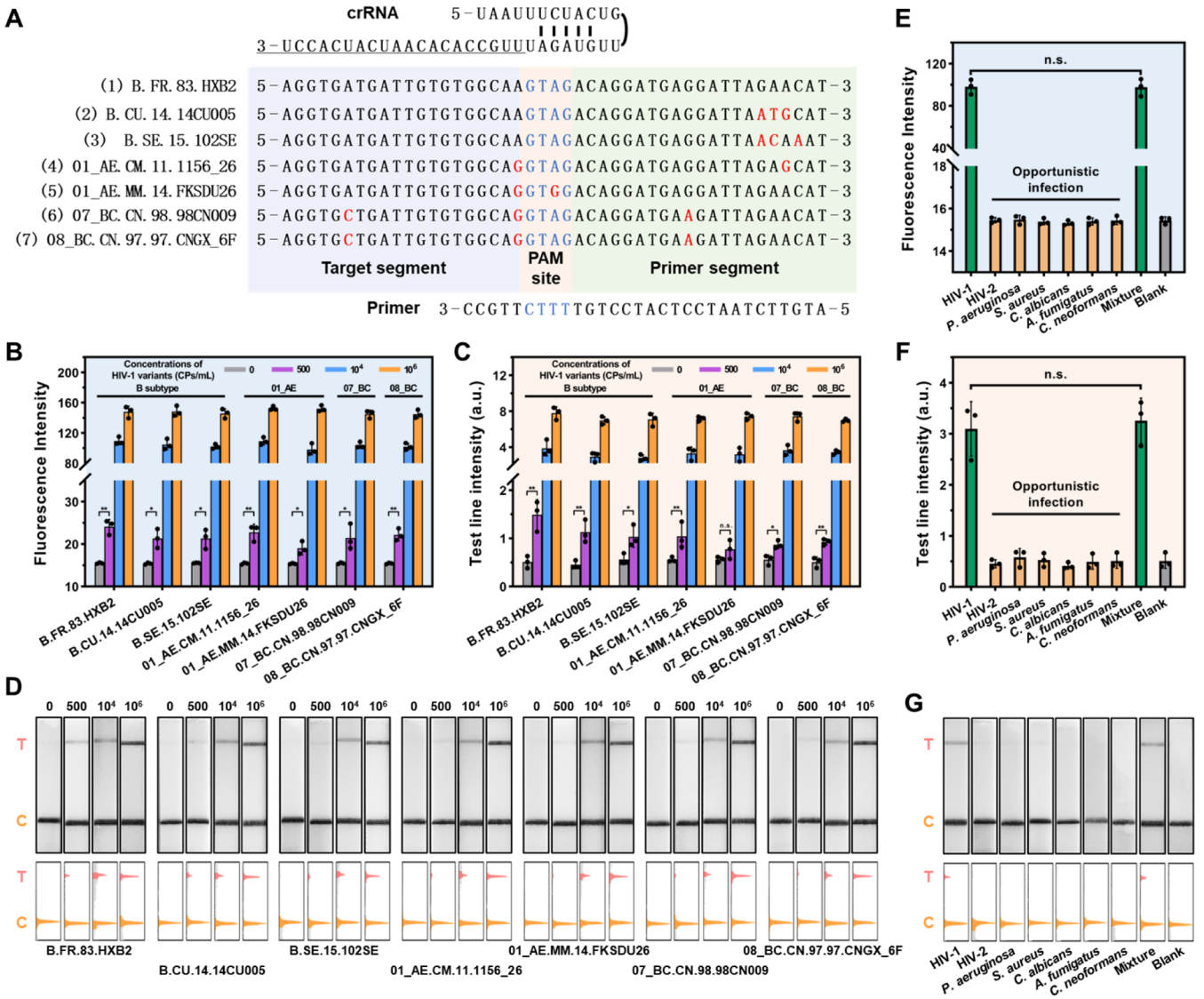


Figure 5. Universality and specificity evaluation of DESCRIBER for HIV-1 detection. (A) Sequence alignment of the standard strain (B.FR.83.HXB2) with common HIV-1 subtypes as well as the mismatches with RT-RPA primers and crRNA utilized in the Cas12a system. (B) Fluorescence intensity measured in each group after 1 h of reaction using the fluorescence assay based on DESCRIBER to evaluate its universality in detecting different subtypes of HIV-1. (C, D) Evaluation of the universality of the test strip assay based on DESCRIBER for HIV-1 detection. (E) Fluorescence intensity measured in each group after 1 h of reaction using the fluorescence assay based on DESCRIBER to evaluate its specificity in detecting HIV-1. (F, G) Evaluation of the specificity of the test strip assay based on DESCRIBER for HIV-1 detection.

dual-mode signal readout methods enhanced the applicability of DESCRIBER in diverse settings, from central laboratories to decentralized community hospitals and homes.

Clinical Application of Dual-Mode DESCRIBER for HIV-1 Diagnosis. HIV-1 is highly variable, and currently, its most prevalent variants include the B subtype and circulating recombinant forms (CRFs) such as 01_AE, 07_BC, and 08_BC. To characterize the universality of DESCRIBER in clinical HIV-1 diagnosis, further evaluations were conducted using simulated genomes representing the above four subtypes. Figure 5A illustrates the mismatches among the simulated genome fragments, the RT-RPA primers, and the crRNA used in the Cas12a system. Usually, RT-RPA exhibited some tolerance to primer mismatches, particularly at the 5′ end, while mismatches at the 3′ end may interfere with primer-template binding and potentially disrupt amplification. Fortunately, mismatches between the R_2 primer and the simulated genomes mainly occur at the 5′ end or in the middle. On the other hand, mismatches between crRNA and the target can affect the *trans*-cleavage activity of Cas12a and impact detection performance, thereby requiring specific characterizations. The detection results, as shown in Figure 5B–D, demonstrated that both the fluorescence assay and the test strip assay effectively identified seven representative sequences from the four subtypes. Although there were slight differences in the signal intensities due to the variations in mismatch severity and positions, the fluorescence assay can still detect these HIV-1 subtypes as low as 500 CPs/mL. The test strip assay only showed a minor effectiveness reduction in detecting 01_AE.MM.14.FKSDU26, but it could still identify this CRF at concentrations higher than 500 CPs/mL.

The HIV-1 patients are susceptible to various pathogens, and these infections are known as opportunistic infections (OIs). To ensure that HIV-1 detection was not compromised,

https://doi.org/10.1021/acs.analchem.4c06066
Anal. Chem. 2025, 97, 3026−3035

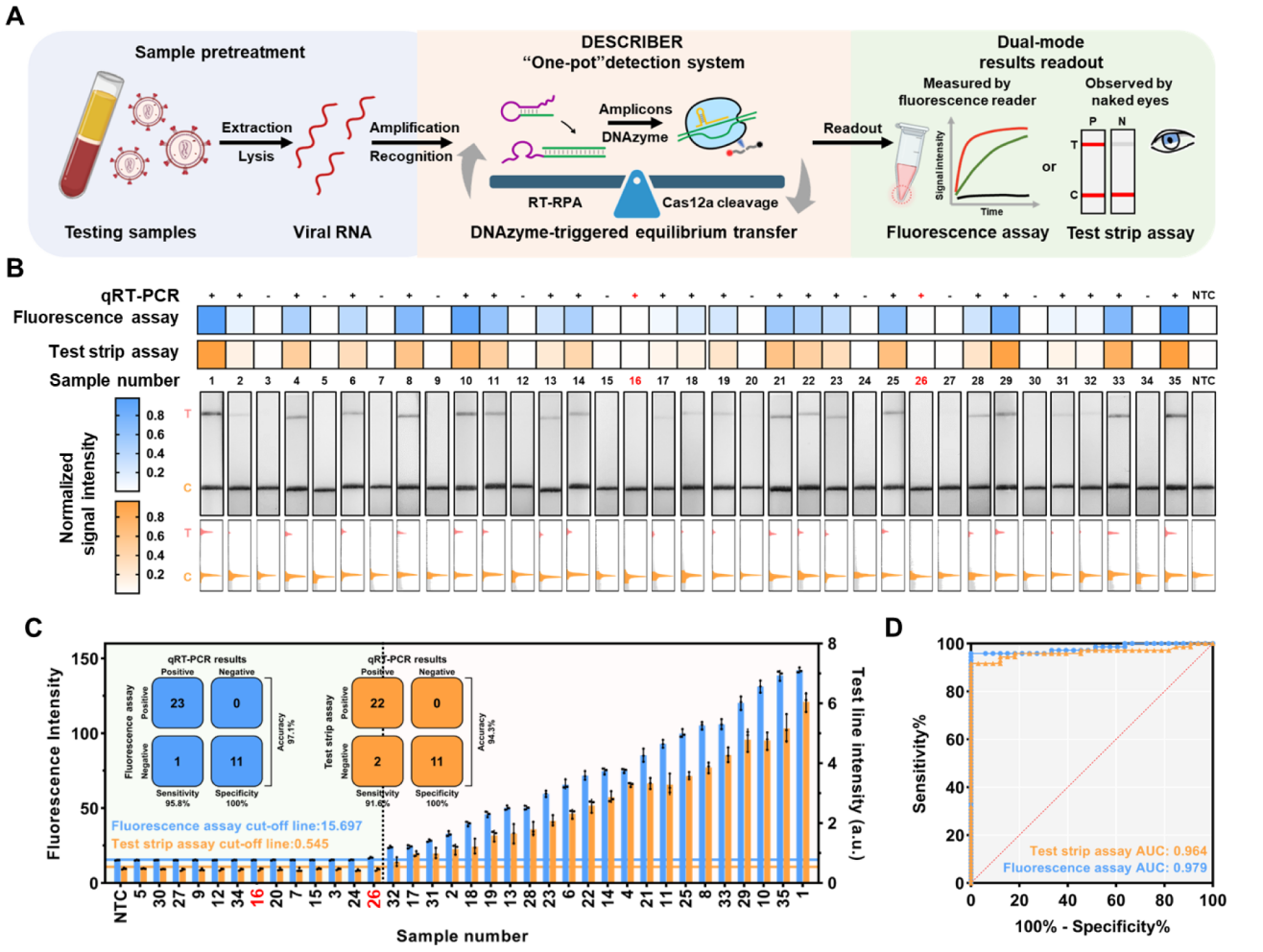


Figure 6. Accuracy evaluation of DESCRIBER for HIV-1 detection and characterization of its clinical potential. (A) Basic workflow of the fluorescence assay and test strip assay based on DESCRIBER for HIV-1 detection. (B) Spiked sample detection by the assays based on DESCRIBER. The "+" and "-" represent positive and negative samples, respectively, as confirmed by qRT-PCR. The heat map represents the values of the fluorescence intensity in the fluorescence assay and the test line intensity as analyzed by ImageJ in the test strip assay. (C) Response of fluorescence intensity and T line intensity vs spiked HIV-1 samples, including 24 positive and 11 negative ones. The average value of signal intensity in the negative control (NTC) plus three times the standard deviation was set as the cutoff line for diagnosis. (D) Receiver operating characteristic curve of the fluorescence assay (blue curve) and test strip assay (orange curve) for HIV-1 detection.

the specificity of DESCRIBER was evaluated against common OI pathogens, including HIV-2 (pseudovirus), invasive fungi (*Candida albicans*, *Aspergillus fumigatus*, and *Cryptococcus neoformans*), and bacteria (*Pseudomonas aeruginosa* and *Staphylococcus aureus*). As shown in Figure 5E−G, neither the fluorescence assay nor the test strip assay produced signals significantly different from the negative control when tested with these OI pathogens, even at concentrations 10 times higher than that of HIV-1 (5000 CPs/mL). Notably, when these OI pathogens were mixed with HIV-1, the detection results showed no significant difference compared with testing HIV-1 alone. These findings demonstrated that the "double-insurance" mechanism of the RT-RPA and CRISPR-Cas12a system ensured the specificity and anti-interference of DESCRIBER in clinical HIV-1 detection.

The accuracy of DESCRIBER was then assessed by analyzing 24 HIV-1 positive samples (10^5−300 CPs/mL) and 11 negative samples (0 CPs/mL), which were prepared by spiking various concentrations of HIV-1 pseudovirus into bovine plasma. Both the fluorescence assay and the test strip assay were used to detect these samples, and their results were compared against qRT-PCR, the "gold standard" in clinical nucleic acid detection. First, a qRT-PCR system for the *pol* fragment was established, which achieved quantitative detection of the HIV-1 genome from 10^6 to 10^2 CPs/mL, and the standard curve was shown in Figure S9 ($Y = -4.158 \times \log_{10}(X) + 46.11$, $R^2 = 0.998$, Y: the Ct values; X: the concentrations of HIV-1 genome (CPs/mL)). This method categorized samples as "negative" if their Ct value exceeded 40 or was undetected; otherwise, they were deemed positive. As a result, qRT-PCR classified all unspiked samples as negative while the average recovery for spiked samples was 88.27%, affirming the overall sample quality (Table S2).

The detection results by the fluorescence assay and test strip assay based on DESCRIBER were exhibited in Figure 6B,C. When using the average value of the negative control (NTC) signal plus three times the standard deviation as the diagnostic cutoff line, only one false-negative result was detected by the fluorescence assay (No. 16) and two by the test strip assay (No. 16 and No. 26). The spiked concentrations of these two samples were 300 and 400 CPs/mL, which were close to the LODs of both DESCRIBER assays but still much lower than

https://doi.org/10.1021/acs.analchem.4c06066
Anal. Chem. 2025, 97, 3026−3035

the threshold for preliminary diagnosis; thus, the potential application of DESCRIBER in HIV-1 screening was theoretically not affected. Based on this criterion, both the fluorescence assay and the test strip assay achieved a specificity of 100% and sensitivities of 95.8% and 91.6%, respectively, resulting in overall accuracies of 97.1% and 94.3%. Additionally, the results shown in Figure 6D demonstrated the reliability of DESCRIBER as a potential diagnostic method for HIV-1, with an area under the curve (AUC) of 0.979 in the fluorescence assay and 0.964 in the test strip assay.

What is more, DESCRIBER demonstrated significant advantages in terms of portability and user-friendliness compared to those of qRT-PCR, as shown in Table S3. DESCRIBER offered clear benefits in terms of reagents, consumables, and instrument costs and provided dual signal readout methods for different detection scenarios, thus lowering the barriers for end users. Compared to the two-step RT-RPA-Cas12a system, the "one-pot" approach in DESCRIBER simplified experimental procedures without compromising detection performance. This streamlined operation reduced the risk of aerosol contamination and held promise for advancing the clinical application of CRISPR-based detection technologies. Unlike other commonly used clinical diagnosis methods for detecting HIV-1 p24 antigen or antibody such as chemiluminescent immunoassay, DESCRIBER targets HIV-1 RNA appearing earlier in the infection period, potentially offering better sensitivity and specificity with a shorter detection window. Furthermore, since the adaptability of RT-RPA and CRISPR-Cas12a systems enables easy and rapid adjustment by updating the primer and crRNA sequences, DESCRIBER offers a practical advantage over immunoassays for detecting diverse nucleic acid targets, which facilitates its expansion into other areas of *in vitro* diagnosis.

CONCLUSIONS

A DNAzyme-triggered equilibrium transfer with a self-activated CRISPR-Cas12a biosensor (DESCRIBER) was established for integrated nucleic acid detection. In this system, C-crRNA silenced Cas12a by its lower affinity and set the initial balance toward RT-RPA. A DNAzyme segment was self-blocked until target nucleic acids triggered its activation during amplification. Then, the activated DNAzyme linearized C-crRNA to guide Cas12a for *trans*-cleavage, facilitating equilibrium transfer without additional driving forces. Dual-mode signal readouts based on fluorescence and test strips were established to meet different needs in different detection scenarios. Both DESCRIBER-based assays showed high sensitivity in detecting HIV-1 genomes, as low as 500 CPs/mL within 1 h. In clinical evaluations, DESCRIBER demonstrated broad applicability in detecting common subtypes and good specificity against opportunistic infection pathogens. Furthermore, DESCRIBER also showed accurate detection of 35 spiked samples, and its performances were comparable to those of the gold-standard qRT-PCR technique. Generally, the proposed strategy herein will aid in the development of versatile and user-friendly CRISPR biosensors for the one-pot assay combined with isothermal nucleic acid amplification technologies and broaden their application scopes in efficient and comprehensive *in vitro* diagnosis.

ASSOCIATED CONTENT

Supporting Information

The Supporting Information is available free of charge at https://pubs.acs.org/doi/10.1021/acs.analchem.4c06066.

Materials, reagents, and oligonucleotides used in this study; detailed experimental procedures; additional optimization and characterization of DESCRIBER; and comparison of methods (PDF)

AUTHOR INFORMATION

Corresponding Authors

Zhinan Xu − *Key Laboratory of Biomass Chemical Engineering of Ministry of Education, College of Chemical and Biological Engineering, Zhejiang University, Hangzhou 310030, China; Institute of Biological Engineering, College of Chemical and Biological Engineering, Zhejiang University, Hangzhou 310030, China; Hangzhou FasTech Biotechnology Company Limited, Hangzhou 310005, China;* orcid.org/0000-0001-7833-026X; Email: znxu@zju.edu.cn

Xiangming Fang − *School of Medicine, Zhejiang University, Hangzhou 310030, China*; Email: xmfang@zju.edu.cn

Authors

Di Huang − *Key Laboratory of Biomass Chemical Engineering of Ministry of Education, College of Chemical and Biological Engineering, Zhejiang University, Hangzhou 310030, China; Institute of Biological Engineering, College of Chemical and Biological Engineering, Zhejiang University, Hangzhou 310030, China;* orcid.org/0000-0002-5611-7158

Yichen He − *Key Laboratory of Biomass Chemical Engineering of Ministry of Education, College of Chemical and Biological Engineering, Zhejiang University, Hangzhou 310030, China; Institute of Biological Engineering, College of Chemical and Biological Engineering, Zhejiang University, Hangzhou 310030, China*

Chutian Xu − *Department of Biomedical Engineering, Boston University, Boston 02215, United States*

Peijie Shen − *Key Laboratory of Biomass Chemical Engineering of Ministry of Education, College of Chemical and Biological Engineering, Zhejiang University, Hangzhou 310030, China; Institute of Biological Engineering, College of Chemical and Biological Engineering, Zhejiang University, Hangzhou 310030, China*

Min Li − *School of Medicine, Zhejiang University, Hangzhou 310030, China*

Mengjun Fang − *Innovation Centre for Child Health, Binjiang Institution of Zhejiang University, Hangzhou 310051, China*

Complete contact information is available at: https://pubs.acs.org/10.1021/acs.analchem.4c06066

Notes

The authors declare no competing financial interest.

ACKNOWLEDGMENTS

This work was financially supported by the National Key Research and Development Program of China (2021YFC2103200), the National Natural Science Foundation of China (22404149), the China Postdoctoral Science Foundation (2023M742994), and the Postdoctoral Fellowship Program of CPSF (GZC20232319). We also acknowledge

Prof. Dr. Xiangcheng Zhu (Center for Future Foods, Muyuan Laboratory) for his valuable comments on this paper.

REFERENCES

(1) Habimana, J. D.; Huang, R.; Muhoza, B.; Kalisa, Y. N.; Han, X.; Deng, W.; Li, Z. *Biosens. Bioelectron.* **2022**, *203*, 114033.
(2) Cong, L.; Ran, F. A.; Cox, D.; Lin, S.; Barretto, R.; Habib, N.; Hsu, P. D.; Wu, X.; Jiang, W.; Marraffini, L. A.; Zhang, F. *Science* **2013**, *339*, 819−823.
(3) Huang, D.; Ni, D.; Fang, M.; Shi, Z.; Xu, Z. *Anal. Chem.* **2021**, *93*, 16965−16973.
(4) Huang, D.; Shen, P.; Xu, C.; Xu, Z.; Cheng, D.; Zhu, X.; Fang, M.; Wang, Z.; Xu, Z. *Biosens. Bioelectron.* **2023**, *222*, 114957.
(5) Xiong, E.; Jiang, L.; Tian, T.; Hu, M.; Yue, H.; Huang, M.; Lin, W.; Jiang, Y.; Zhu, D.; Zhou, X. *Chem. Int. Ed. Engl.* **2021**, *60*, 5307−5315.
(6) Harrington, L. B.; Burstein, D.; Chen, J. S.; Paez-Espino, D.; Ma, E.; Witte, I. P.; Cofsky, J. C.; Kyrpides, N. C.; Banfield, J. F.; Doudna, J. A. *Science* **2018**, *362*, 839−842.
(7) Swarts, D. C.; Jinek, M. *Mol. Cell* **2019**, *73*, 589−600.
(8) Yamano, T.; Nishimasu, H.; Zetsche, B.; Hirano, H.; Slaymaker, I. M.; Li, Y.; Fedorova, I.; Nakane, T.; Makarova, K. S.; Koonin, E. V.; Ishitani, R.; Zhang, F.; Nureki, O. *Cell* **2016**, *165*, 949−962.
(9) Lei, L.; Yan, S.-Y.; Yang, R.; Chen, J.-Y.; Li, Y.; Bu, Y.; Chang, N.; Zhou, Q.; Zhu, X.; Li, C.-Y.; Xiong, J.-W. *Nucleic Acids Res.* **2017**, *45* (6), 3422−3436.
(10) Chen, J. S.; Ma, E.; Harrington, L. B.; Costa, M. D.; Tian, X.; Palefsky, J. M.; Doudna, J. A. *Science* **2018**, *360*, 436−439.
(11) Li, S.-Y.; Cheng, Q.-X.; Wang, J.-M.; Li, X.-Y.; Zhang, Z.-L.; Gao, S.; Cao, R.-B.; Zhao, G.-P.; Wang, J. *Cell Discovery* **2018**, *4* (1), 20.
(12) Huang, D.; Qian, J.; Shi, Z.; Zhao, J.; Fang, M.; Xu, Z. *Biol* **2020**, *9*, 3114−3123.
(13) Shen, P.; Si, Z.; Huang, D.; Xu, Z.; Wang, Z.; Fang, M.; Xu, Z. *Analyst* **2023**, *148*, 2573−2581.
(14) Feng, W.; Peng, H.; Xu, J.; Liu, Y.; Pabbaraju, K.; Tipples, G.; Joyce, M. A.; Saffran, H. A.; Tyrrell, D. L.; Babiuk, S.; Zhang, H.; Le, X. C. *Anal. Chem.* **2021**, *93*, 12808−12816.
(15) Wu, H.; Chen, Y.; Shi, Y.; Wang, L.; Zhang, M.; Wu, J.; Chen, H. *Biosens. Bioelectron.* **2021**, *178*, 113001.
(16) Chen, Y.; Shi, Y.; Chen, Y.; Yang, Z.; Wu, H.; Zhou, Z.; Li, J.; Ping, J.; He, L.; Shen, H.; Chen, Z.; Wu, J.; Yu, Y.; Zhang, Y.; Chen, H. *Biosens. Bioelectron.* **2020**, *169*, 112642.
(17) Ding, X.; Yin, K.; Li, Z.; Lalla, R. V.; Ballesteros, E.; Sfeir, M. M.; Liu, C. *Nat. Commun.* **2020**, *11* (1), 4711.
(18) Hu, F.; Liu, Y.; Zhao, S.; Zhang, Z.; Li, X.; Peng, N.; Jiang, Z. *Biosens. Bioelectron.* **2022**, *202*, 113994.
(19) Huang, D.; Zhao, Y.; Fang, M.; Shen, P.; Xu, H.; He, Y.; Chen, S.; Si, Z.; Xu, Z. *Lab Chip* **2023**, *23*, 4265−4275.
(20) Chen, Y.; Zong, N.; Ye, F.; Mei, Y.; Qu, J.; Jiang, X. *Anal. Chem.* **2022**, *94*, 9603−9609.
(21) Li, Z.; Uno, N.; Ding, X.; Avery, L.; Banach, D.; Liu, C. *ACS Nano* **2023**, *17*, 3966−3975.
(22) Yin, K.; Ding, X.; Li, Z.; Zhao, H.; Cooper, K.; Liu, C. *Anal. Chem.* **2020**, *92*, 8561−8568.
(23) Lin, M.; Yue, H.; Tian, T.; Xiong, E.; Zhu, D.; Jiang, Y.; Zhou, X. *Anal. Chem.* **2022**, *94*, 8277−8284.
(24) Uno, N.; Li, Z.; Avery, L.; Sfeir, M. M.; Liu, C. *Anal. Chim. Acta* **2023**, *1262*, 341258.
(25) Kang, W.; Xiao, F.; Zhu, X.; Ling, X.; Xie, S.; Li, R.; Yu, P.; Cao, L.; Lei, C.; Qiu, Y.; Liu, T.; Nie, Z. *Angew. Chem., Int. Ed.* **2024**, *63* (16), No. e202400599.
(26) Hu, M.; Qiu, Z.; Bi, Z.; Tian, T.; Jiang, Y.; Zhou, X. *Proc. Natl. Acad. Sci. U.S.A.* **2022**, *119* (26), No. e2202034119.
(27) Hu, M.; Liu, R.; Qiu, Z.; Cao, F.; Tian, T.; Lu, Y.; Jiang, Y.; Zhou, X. *Chem. Int. Ed. Engl.* **2023**, *62* (23), No. e202300663.
(28) Liu, P.; Lin, Y.; Zhuo, X.; Zeng, J.; Chen, B.; Zou, Z.; Liu, G.; Xiong, E.; Yang, R. *Angew. Chem., Int. Ed.* **2024**, *63* (23), No. e202401486.
(29) Lu, S.; Tong, X.; Han, Y.; Zhang, K.; Zhang, Y.; Chen, Q.; Duan, J.; Lei, X.; Huang, M.; Qiu, Y.; Zhang, D. Y.; Zhou, X.; Zhang, Y.; Yin, H. *Nat. Biomed. Eng.* **2022**, *6*, 286−297.
(30) Chen, Y.; Xu, X.; Wang, J.; Zhang, Y.; Zeng, W.; Liu, Y.; Zhang, X. *Anal. Chem.* **2022**, *94*, 9724−9731.
(31) Wu, N.; Willner, I. *Nano Lett.* **2016**, *16*, 2867−2872.
(32) Wu, Y.; Chang, D.; Chang, Y.; Zhang, Q.; Liu, Y.; Brennan, J. D.; Li, Y.; Liu, M. *Small* **2023**, *19* (41), 2303007.

https://doi.org/10.1021/acs.analchem.4c06066
Anal. Chem. 2025, 97, 3026−3035